Stop-Flow SEOP Polarizer for ^{129}Xe

T. Pałasz[a,*], L. Mikowska[a], B. Głowacz[a], Z. Olejniczak[b], M. Suchanek[c], and T. Dohnalik[a]

[a]Marian Smoluchowski Institute of Physics, Jagiellonian University, Łojasiewicza 11, PL-30348 Kraków, Poland
[b]Institute of Nuclear Physics, Polish Academy of Sciences, Radzikowskiego 152, PL-31342 Kraków, Poland
[c]Department of Physics, University of Agriculture, Mickiewicza 21, PL-31120 Kraków, Poland

(Received Received October 1, 2019; in final form October 23, 2019)

In the view of growing application of hyperpolarized xenon in various fields of science and medicine, the availability of relatively low cost, reliable polarizers is of the utmost importance. The article describes the design and construction of the spin exchange optical pumping (SEOP) polarizer for ^{129}Xe, operating in the stop-flow mode. Using 9 W of laser power at the input of 1 litre optical pumping cell, a single batch of the gas mixture is polarized in about 15 minutes. The xenon nuclear polarization is calibrated against the thermally polarized water and xenon phantoms. It reaches about 40 % in the gas mixture containing 3 % of isotopically enriched xenon. The hyperpolarized xenon is accumulated in the detachable liquid nitrogen dewar containing 0.6 T Halbach magnet with the cold trap inside. All components that are important for the effective operation of the system are described in detail, and possible improvements are pointed out.

DOI: 10.12693/APhysPolA.136.1008

PACS/topics: Magnetic resonance imaging, nuclear hyperpolarization, spin exchange optical pumping, xenon-129

1. Introduction

The unique properties of hyperpolarized ^{129}Xe gas have been explored in the fields of physics, chemistry, biology, and medicine, as reported in recent excellent books [1–3] and review papers [4–6]. First of all, although xenon as a noble gas is chemically inactive, ^{129}Xe chemical shift range as observed in the NMR spectroscopy is very large, due to its high sensitivity to chemical environment. This feature has been used in material science and chemistry, for example in studying porous materials [7]. Second, by inhaling HP xenon gas, high resolution MR images of human lungs can be obtained, providing structural information that is inaccessible by other techniques, like proton MRI, and CT. This led to the development of very sensitive diagnostic methods for asthma, COPD, cystic fibrosis, and other lung diseases [8]. Moreover, dynamic ventilation studies can be performed. In this particular application, ^{129}Xe has successfully replaced ^{3}He, which is nowadays used to smaller extent due to its extremely high cost [9]. Third, in contrast to ^{3}He, ^{129}Xe is soluble in blood, opening interesting possibilities to use it as a contrast agent in perfusion studies [10], and in magnetic resonance imaging of various organs, including human brain [11–12].

In all these applications, it is necessary to increase sensitivity by hyperpolarizing ^{129}Xe, in order to compensate low gas density. The most popular method to achieve this is the Spin Exchange Optical Pumping (SEOP) [13–15]. Several designs of the SEOP ^{129}Xe polarizers are reported in the literature [16–20]. Commercial ^{129}Xe polarizers are also available [21–22]. In order to produce large amounts of polarized xenon, they operate either in a single cycle mode, using large optical pumping cells, or in a continuous flow mode, with consecutive xenon accumulation. Both approaches require a high-power laser to be used, of the order of several tens of watts or more, and a sophisticated optical setup. Typical polarization levels achieved are in the range 35–45 % at the production rate of a few litres of gas per hour.

This article describes the design and implementation of the low cost, stop-flow ^{129}Xe polarizer using the SEOP method. It operates at the 3–6 % xenon concentration in the gas mixture. One-litre optical pumping cell containing a rubidium droplet and a mixture of xenon and buffer gases is heated to 120–140 °C and irradiated by 9 W laser light, producing in a single cycle 30–60 cm^3 of polarized xenon in 10–15 minutes. Then the hyperpolarized xenon is separated from the buffer gases and stored in the liquid nitrogen cold finger. Five cycles are necessary to provide about 300 cm^3 of hyperpolarized xenon for imaging purposes.

2. Hyperpolarization of ^{129}Xe via the SEOP process

Polarization of atoms with nuclear spin one-half, including hydrogen atoms, which are a typical source of NMR signal in medical imaging, is defined by:

$$P = \frac{N_\downarrow - N_\uparrow}{N_\uparrow + N_\downarrow}, \tag{1}$$

where $N_\uparrow$ and $N_\downarrow$ are the populations of nuclei in the higher and lower energetic states respectively. In thermal equilibrium, the application of the Boltzmann law leads to the following approximate formula for the nuclear polarization:

*corresponding author; e-mail: tadeusz.palasz@uj.edu.pl

$$P \cong \frac{\hbar\gamma B}{2k_{\mathrm{B}}T}, \tag{2}$$

where $\hbar$ is the Planck constant, γ gyromagnetic ratio, B magnetic field induction, k_{B} the Boltzmann constant and T temperature in Kelvin. In $B = 1.5$ T at the human body temperaturethe formula gives rather low proton polarization of $\sim 5 \times 10^{-6}$. Nevertheless, in the case of highly hydrated tissues, this is compensated by high concentration of hydrogen nuclei. The problem arises when thin and low-moisture lung parenchyma is to be imaged. Therefore, the idea of using hyperpolarized noble gases (^{3}He or ^{129}Xe) for lung imaging was conceived [23–26]. Hyperpolarization of ^{129}Xe gas obtained via SEOP method, exceeds the thermal value by almost five orders of magnitude.

The SEOP process takes place in a glass optical pumping cell (OP), which is placed in a low magnetic field, to remove the degeneracy of electronic hyperfine states. A droplet of rubidium is put into the OP cell, which is filled with a mixture of xenon and buffer gases (^{4}He and N_2), at proper proportions. The OP cell is heated to about 120 °C, to evaporate rubidium. A high-power laser operating at the basic optical transition of rubidium (D_1, 794.7 nm), produces a circularly polarized beam that irradiates the entire volume of the OP cell. A high nuclear polarization of ^{129}Xe is obtained in a two-stage process. First, a selected electronic state of rubidium is optically pumped, by transferring the angular momentum of circularly polarized photons to the rubidium valence electrons. Then the electron spin orientation is transferred to ^{129}Xe nuclei by collisions. Depending on the physical conditions created in the OP cell (such as the partial pressures of individual gases), two mechanisms can be responsible for this process: binary Rb–Xe collisions or three-body Rb–Xe–N_2 collisions leading to the creation of the van der Waals Rb–Xe molecules [27]. The latter is much more efficient, the Fermi contact interaction appearing in the van der Waals molecule being the preferred spin transfer channel. The following collision with the N_2 molecule breaks down the van der Waals molecule into atoms. The nitrogen gas plays an additional role, causing a non-radiative relaxation of rubidium atoms from the excited state to the ground state, thus avoiding the resonance emissions of D_1 photons at random directions and polarizations that would disturb the optical pumping process. The efficiency of the optical pumping process can be further enhanced by the addition of ^{4}He gas to the OP cell, through the process of collisional mixing (^{4}He atoms colliding with excited rubidium atoms). Buffer gases, especially helium, increase the pressure in the OP cell and cause the absorption line to widen. As a result, more photons can be absorbed in the optical pumping process.

The optimization of the SEOP process relies on the appropriate choice of several experimental parameters. They include the composition of the gas mixture in the OP cell [28–30], its operating temperature, volume of the optical pumping cell [31–33] and the laser power [34]. Moreover, since the natural abundance of the spin one-half xenon isotope is only 26.44 %, it is preferred to use an isotopically enriched medium, with the ^{129}Xe content exceeding 85 %. The efficiency of the SEOP process can be described by the achieved final nuclear polarization of ^{129}Xe, the time necessary to reach it (the build-up time), and the amount of hyperpolarized gas that can be extracted from the OP cell for further use.

3. Apparatus

The presented SEOP ^{129}Xe polarizer operates in the low pressure regime, in the stop — flow mode. The block diagram of the polarizer is shown on Fig. 1. The central part of the device is a glass cylindrical OP cell, in which the SEOP process takes place. A drop of rubidium metal is put into OP cell in the inert atmosphere of argon or nitrogen, before installing it inside the polarizer.

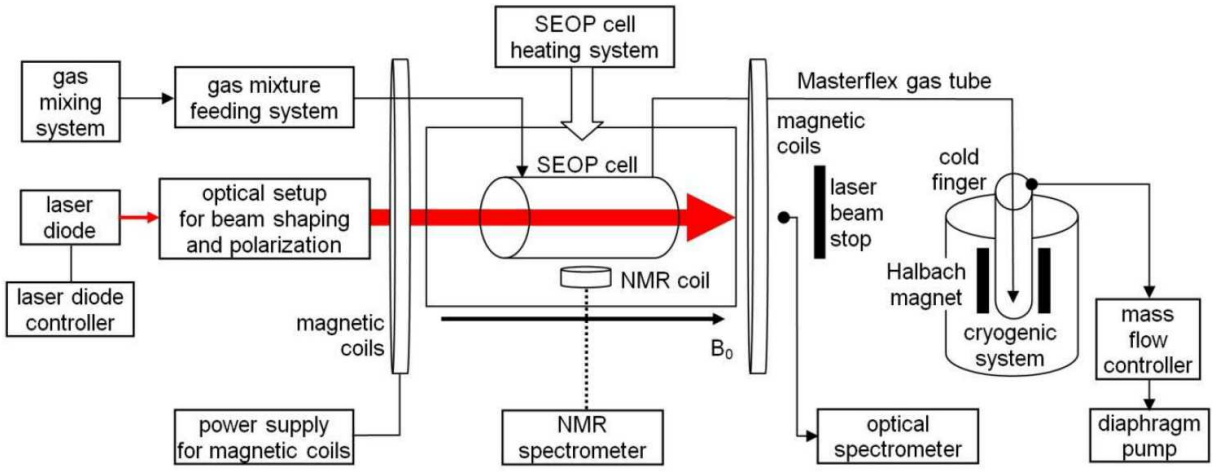

Fig. 1. Basic functional blocks of the polarizer.

Then the OP cell is filled with the prepared mixture of xenon and buffer gases by a gas dosing system, through a stainless steel tubing. The pressure in the OP cell is controlled by a gas regulator. A non-magnetic thermally isolated chamber equipped with the hot air circulation system holds the OP cell, controlling its temperature, thus producing rubidium vapor of required pressure inside the cell. The magnetic field of 3.6 mT with homogeneity of the order of 1 % in the region of OP cell is generated by eight square-shaped coils surrounding the heating chamber, and stabilized to better than 0.1 %. Rubidium is optically pumped by the circularly polarized laser beam, which is tuned to the rubidium D_1 line of 794.7 nm, and shaped by a specially designed optical system, to assure the irradiation of the entire OP cell. A precise optical spectrometer with diffraction grating and the CCD detector equipped with the fiber optic input controls the laser tuning and measures the absorption of the laser beam.

The xenon nuclear polarization is measured by a small surface coil attached to the OP cell and interfaced to the modified pulse NMR spectrometer (Aurora, Magritek). When the polarization reaches the steady state, the gas mixture is transferred via the flexible, non-depolarizing tube (Masterflex) to the liquid nitrogen cryogenic system. This separates xenon from and buffer gases. A four-stage diaphragm pump removes the non-frozen buffer gases (helium and nitrogen) from the cold finger. The electronically controlled mass flow controller maintains a constant flow of buffer gases pumped out of the cold finger, which is critical owing to the decreasing pressure in the OP cell during transfer. The solid polarized xenon is stored and accumulated in the cold trap that is placed in the permanent Halbach magnet and submerged in liquid nitrogen. The alignment of the HP xenon transferring route with respect to magnetic field is optimized to reduce depolarization effects.

All components are mounted on a non-magnetic frame consisting of aluminum closed profiles (Rexroth system, Bosch). Additionally, a turbomolecular pump is used for initial cleaning of the OP cell and the gas supply system (not shown). The principal components of the polarizer are described in more details in the following subsections.

3.1. Optical Pumping cell

Preliminary experiments of the SEOP process were performed in a large OP cell of 6 litres and produced insufficient nuclear polarization, due to limited laser power [35]. Therefore a smaller OP cell was designed. It is a bone-shaped Pyrex tube of 5.6 cm inner diameter and 41 cm length, resulting in the 1010 cm^3 internal volume. The input and output optical windows (without any anti-reflective cover) have larger diameter of 6.3 cm to avoid laser beam distortions that might be caused by deformations of the glass surface created in the process of connecting with a glass tube. Two stopcocks (Teflon valves, Rotaflo) with gas connectors are installed at the distances of about 5 cm from the ends of the cylinder. They are equipped with special threads for mounting the Masterflex gas tubes, which allows an easy OP cell replacement in the case of contamination. Initially, the OP cell is thoroughly cleaned and put into the glove box that is filled with argon. Approximately 0.5 g of metallic rubidium is heated to about 50 °C, and after removing the Teflon part of the Rotaflo valve it is dripped into the OP cell.

3.2. Heating system

In order to get the required rubidium vapor pressure inside the OP cell, it is necessary to heat it to the temperature in the 100–140 °C range. However, the valves equipped with the teflon sealing, as well as plastic Masterflex tubes should be kept at ambient temperature. For that purpose, a thermally isolated heating chamber in the form of aluminum box (19 cm height, 31 cm width, and 53 cm length) was constructed. The inner surface of the chamber is covered by mineral wool for thermal insulation. The inlet and outlet of the heating chamber are connected to the closed air circulation circuit by 10 cm inner diameter flexible airflow tubes also isolated with mineral wool. The air circulation system is powered by the 2 kW electric heater and the centrifugal fan. The NTC thermistor installed close to the OP cell is used to measure temperature, and the PID controller (Selec, model PID500) stabilizes it with 0.1 °C accuracy. The heating chamber is equipped with optical windows (100 mm diameter, 80 mm clear aperture) for the input and output of the 6 cm diameter laser beam. These optical windows have an anti-reflective coating at 795 nm (Eksma Optics, Lithuania).

3.3. Magnetic field generation

The magnetic field is generated by a set of eight coils that are wound on the square (43 cm side) supports with optimized number of turns and their positions [35]. The coils are divided into three sections (3+2+3), which are supplied by three independent current sources providing 5.11 A, 4.80 A, and 5.11 A, respectively, with 10 mA accuracy. Each coil in subsequent pairs, counting from the center of the system, have 80, 92, 102 and 116 turns, respectively. The distances between individual coils as measured from the geometrical center are 66, 210, 382 and 520 mm. The achieved magnetic field homogeneity is better than 1 % in the OP cell region. The magnetic induction of 3.6 mT corresponds to the ^{129}Xe resonance frequency equal to 42.4 kHz, which was chosen to be far from any interfering RF noise.

3.4. Laser, beam expander and polarization optics

A high power narrowband laser beam that is precisely tuned to the electronic transition of rubidium is required for the SEOP process. The best choice for this task is a laser diode array (LDA), which consists of a set of semiconductor laser diodes mounted on a common heat sink [36–38]. The industry standard for the near infrared LDA laser is the 19-diode bar with 150 μm emitter width,

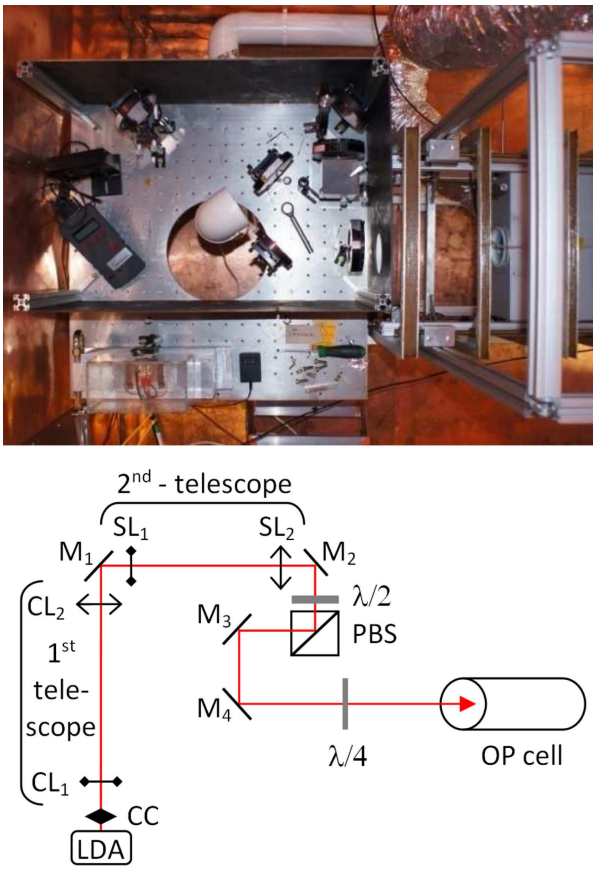

Fig. 2. Picture (top) and scheme (bottom) of the laser setup with beam shaping and polarization optics. LDA — Laser Diode Array; CC — cylindrical collimator; CL_1 and CL_2 — concave and convex cylindrical lenses; SL_1 and SL_2 — concave and convex spherical lenses; M_1,M_2, M_3, M_4 — mirrors; PBS — polarizing beam splitter, $\lambda/2$ and $\lambda/4$ — half-wavelength and quarter-wavelength plates.

500 μm pitch and 6 degrees divergence angle [39–40]. The commercial LDA (M1B-794.7[0.6]-35C-VBG, DILAS) is used, generating the laser beam of 794.7 nm wavelength (D_1 rubidium transition) with the 0.9 nm FWHM (full width at half maximum). The LDA is equipped with the Volume Bragg Gratings (VBG) resonator which reduces the bandwidth and stabilizes the wavelength. The LDA heat sink is mounted on a copper radiator. Two Peltier coolers controlled by homemade PID circuits and installed between the radiator and the water cooled aluminum block stabilize the LDA temperature to better than 0.1 °C. This satisfies the required heat sink capacity for maximum 30 W of optical output power, assuming 42 % efficiency of LDA. The LDA is controlled by the commercial laser diode driver, supplying maximum 60 A (Ekspla). The optical setup is shown on Fig. 2.

The LDA has been factory equipped with a cylindrical collimator (CC), focusing the fast axis of the LDA emitters. In order to fit the laser beam profile to the geometry of the OP cell, two refracting telescopes for the beam collimation and expansion are used. The first telescope increases 20 times the diameter of the collimated LDA beam in the fast axis direction, using two cylindrical lenses: the plano-concave ocular CL_1 and plano-convex telescope lens CL_2, with the focal lengths of −25 mm and +500 mm, respectively. The second telescope expands 4.5 times the beam diameter using two spherical lenses: the bi-concave ocular SL_1 and bi-convex telescope lens SL_2, with the focal lengths of −200 mm and +500 mm, respectively. The LDA produces beam with 20:1 linear polarization. The expanded beam (with light intensity lower than 1 W/cm^2) passes the $\lambda/2$ plate, which rotates the direction of linear polarization. The linearity of the beam is further improved by the polarizing beam splitter cube (PBS). The beam passes the cube perpendicularly, so that only *s*-polarized beam leaves PBS. Finally, the linearly polarized beam is circularly polarized by the $\lambda/4$ plate. The optical system uses four dielectric mirrors, the last two of which serve to direct the pumping beam along the cylindrical axis of the OP cell. All lenses and multi-order plates were made by Eksma Optics and have anti-reflection coatings at 795 nm.

An optical spectrometer is used for measuring the light absorption in the OP cell and for final tuning the LDA to atomic transition (USB HR 4000, Ocean Optics, with 1800 lines/mm diffraction grating and 25 μm slit).

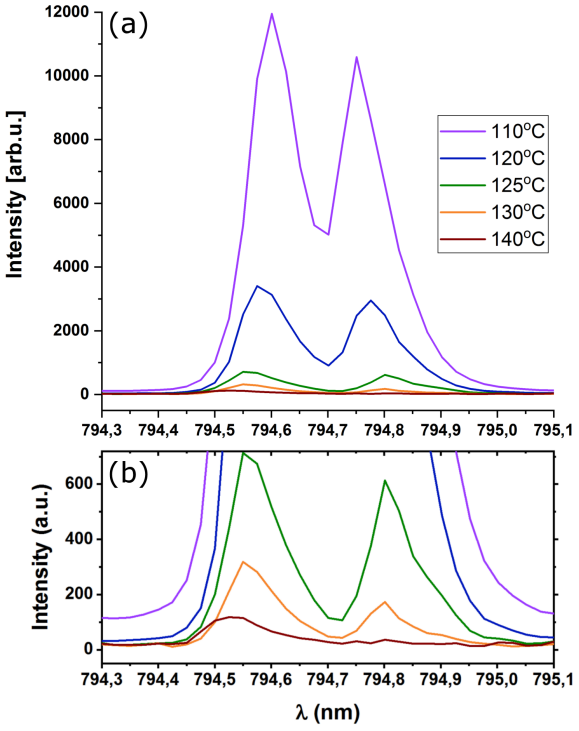

Fig. 3. Spectra of the pumping beam after passing through the OP cell (a, b). At higher temperatures of the OP cells, the pumping beam is strongly absorbed. Spectra for temperatures above 120 °C are shown in part (b), in an enlarged vertical scale.

The multimode fiber installed behind the output window of the heating chamber collects the laser light that passed through the OP cell and transmits it to the slit of the spectrometer. The optimized laser beam forming system allowed for uniform illumination of the input window of the OP cell. With an LDA emission of about 16 W, 9 W were obtained at the OP cell input. The high density of the rubidium vapor inside the heated OP cell makes almost all light of the pumping beam (tuned to the absorption line D_1 and widened additionally as a result of collisions with helium atoms) absorbed. The examples of temperature dependent partially absorbed pumping beam spectra are shown in Fig. 3.

3.5. Gas mixture preparation

The SEOP process is carried out in a mixture of three gases: xenon, helium and nitrogen in the presence of rubidium vapor. The polarizer operates in the stop-flow mode, with a portion of prepared gas mixture supplied to the OP cell at the desired pressure of 1.25 bar. The concentration of the xenon gas which is ^{129}Xe isotope enriched to 91% (Messer) ranges from 3 to 6 %. It is sufficient to obtain from 30 to 60 cm^3 of hyperpolarized medium under normal pressure in a single cycle of polarization.

The gas mixing system is shown on Fig. 4. It consists of three high-pressure cylinders equipped with precise, two-stage reducers. All reducers end with Swagelok connectors for 6 mm diameter and 1 mm thick stainless, electropolished 316 steel tubes, which are used for all necessary connections. The needle valves (Hooke) of helium leakage class are used for the gas flow control. A high-efficiency turbo-molecular pump with a scroll prepump (TPS Compact, Varian) is used for initial evacuation. All interconnections of the gas handling components are made with the Swagelok standard, ensuring tightness and a high degree of gas purity. High purity (Class 6.0) nitrogen and helium buffer gases are stored in CYL_1 and CYL_2, respectively, while CYL_3 stores isotopically enriched xenon. The desired gas mixture is prepared in CYL_4, which is switched between two positions. In the position drawn in the solid line and marked as [F], it is filled successively with xenon, helium, and nitrogen through the mechanical 0.5 μm micro filter, until it reaches the pressure of 9 bar. In the position drawn in the dashed line and marked as [D], the CYL_4 bottle feeds the gas mixture to the OP cell through the precision reducer PR_4 and the NV_7 needle valve. Since CYL_4 has 1 liter volume, the prepared portion of the gas mixture is sufficient to perform nine polarization cycles in the 1 litre OP cell, resulting in 270 to 540 cm^3 of polarized xenon under atmospheric pressure.

3.6. Xenon cold trap

After completing the polarization cycle, the OP cell is drawn off at the constant flow rate by a 4-stage diaphragm pump. A mass flow controller that is installed at the inlet of the pump (F-202-AV-M10-PGD-88-V, Bronkhorst) allows to adjust the gas flow rate in the 7 to 15 scc/min range (scc — standard cubic centimetres),

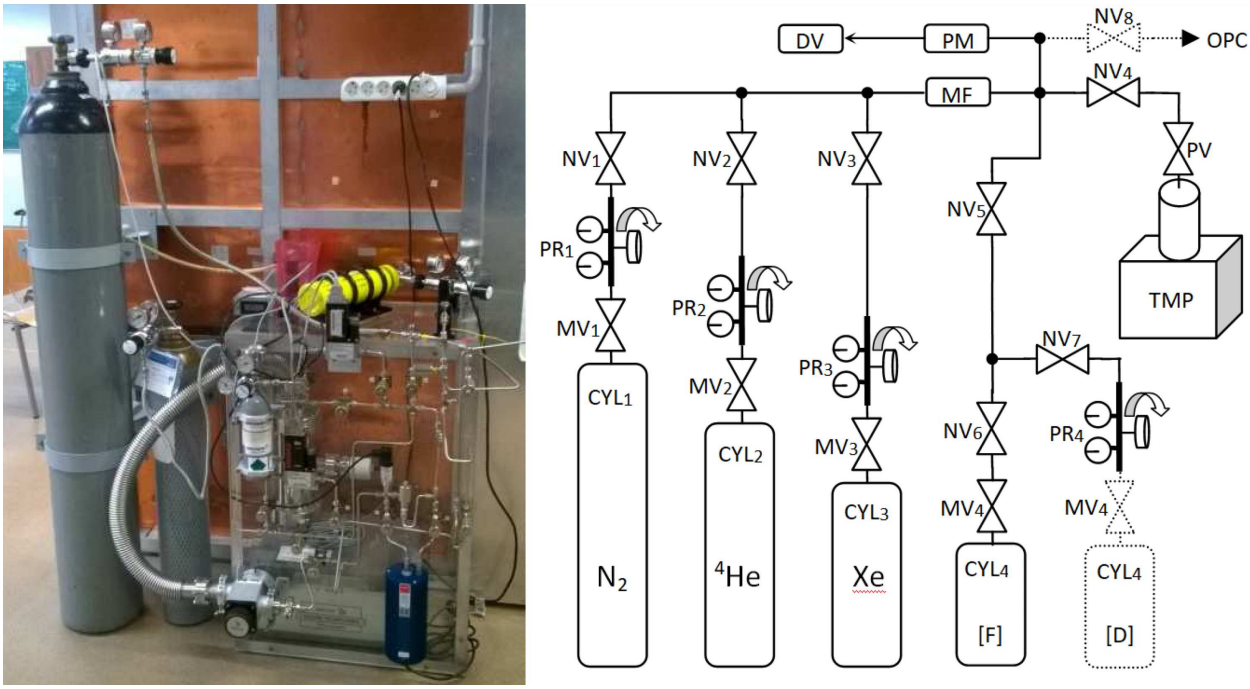

Fig. 4. Picture (left) and scheme (right) of gas handling system. CYL_{1-4} — gas cylinders, MV_{1-4} — main valves, PR_{1-4} — precision reducers, NV_{1-8} — needle valves, MF — micro-filter, PM — precise pressure meter, DV — digital voltmeter, PV — pump valve, TMP — turbo molecular pump; OPC — gas connector to the OP cell.

emptying the OP cell in 120 to 60 s. The gas mixture passes through the cold finger that is immersed in liquid nitrogen, where the xenon freezes, while the remaining gases are pumped out. A commercial 26 mm outer diameter cold finger made by Sigma–Aldrich is used.

In order to preserve the nuclear polarization of frozen xenon during storage and accumulation process, it is necessary to keep it in a high magnetic field, of the order of hundreds mT [41]. A permanent magnet with the Halbach structure was constructed for that purpose, using the N42 type NdFeB magnets of $20 \times 20 \times 50$ mm^3 dimensions, characterized by 915 kA/m coercive field strength [42, 43]. The Halbach structure was simulated by the finite element method, using the FEMM program [44], and the results are shown on Fig. 5 (left).

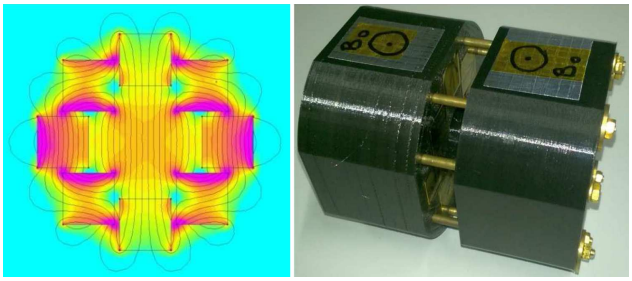

Fig. 5. Simulation results of the Halbach structure (left); magnet during assembling (right).

The assumed internal bore diameter was equal to 30 mm, and the total magnet length 100 mm. Colored maps indicate the values of magnetic field induction in a 200 mT (green) to 830 mT (violet) scale. The magnetic induction is about 600 mT, with homogeneity better than 10 % in the region of the cold finger, which has 23 mm internal diameter. Two identical Halbach structures were combined to obtain the magnet of 100 mm total length. The magnet supports made from the PLA material were printed on a 3D printer. Both structures were connected by 8 brass rods threaded at the ends. The structures were compressed together (overcoming the repulsive force of the magnets) by successive tightening the nuts at the ends of the brass rods. The process of assembling the magnets is shown in the Fig. 5 (right). The Halbach magnet with the cold finger inside is put into 5 litre liquid nitrogen dewar. When the accumulation of the frozen xenon is complete, the dewar can be transported to the final destination, where polarized xenon can be thawed. The polarization loss during the whole procedure including 30 min transport time, is of the order of 50%.

4. NMR signal measurements and calibration of xenon polarization

The polarization process is monitored by a dedicated NMR system. A square 50×50 mm^2 RF surface coil made of 80 turns attached to the central part of the OP cell is tuned to 42 kHz and interfaced to the Aurora NMR spectrometer (Magritek). The free induction decay (FID) signal excited by a single RF pulse is directly sampled and recorded using the Prospa program (Magritek). The NMR spectrometer is supplemented by an active Q-spoiling circuit, reducing the RF coil ringing time from 12 ms to 1.5 ms. Since the NMR monitoring system probes only about 15 % of the OP cell volume, it does not interfere with the polarization process.

In order to determine the absolute value of xenon polarization, the same setup was used to measure the NMR signal from the premagnetized water phantom of geometry that was matched to the OP cell. It was put in the OP cell place for the purpose of calibration. The B_0 magnetic field was reduced by the $\gamma_{\mathrm{Xe}}/\gamma_p$ factor, so that the resonance frequencies for xenon and hydrogen were equal. The 90° RF pulse length was reduced accordingly. Since the same RF coil was used, all experimental parameters affecting the NMR signal intensity, such as the measured volume, RF coil quality factor, and the receiver sensitivity were identical.

The NMR signal from the thermally polarized water phantom was rather weak, so that its accumulation would be necessary to achieve sufficient accuracy of the calibration procedure. However, the fluctuations of the B_0 magnetic field cause the FID phase to be unstable, making the averaging procedure unfeasible. Therefore, the water phantom was premagnetized using an additional cylindrical coil that produced a pulse magnetic induction $B_{\mathrm{in}} = 16.95$ mT. The coil is switched on for a certain period of time, such that the water sample polarization reaches equilibrium. Then it is switched off, and the NMR signal is measured after the magnetic field returns to its equilibrium B_0 value.

The relaxation processes of water in the fields $B_{\mathrm{tot}} = B_0 + B_{\mathrm{in}} = 17.9$ mT and $B_0 = 1$ mT are shown in Fig. 6a and b, and the determined T_1 times were equal to (2.9 ± 0.2) s and (2.5 ± 0.4) s, respectively. Based on these measurements, the prepolarization time was set to 9 s, and the second parameter enters the Eq. 3 for the absolute xenon polarization as $T_{1,p}$, to correct for the relaxation in the interval $\delta t = 100$ ms between switching B_{in} off and applying the RF pulse.

The absolute value of xenon polarization P_{Xe} was calculated from the following formula [17], modified by an additional factor that takes into account the relaxation of water in B_0 during δt:

$$\frac{S_{\mathrm{Xe}}}{S_p} = \frac{P_{\mathrm{Xe}}}{P_p}\,\frac{N_{\mathrm{Xe}}\,\beta_{129}}{N_p}\,\frac{\gamma_{\mathrm{Xe}}}{\gamma_p} \times \frac{\exp\left(-t_{\mathrm{del}}/T^*_{2,\mathrm{Xe}}\right)}{\exp\left(-t_{\mathrm{del}}/T^*_{2,p}\right)\exp\left(-\delta t/T_{1,p}\right)}, \tag{3}$$

where S_{Xe}, S_p are the signal intensities of xenon and water, respectively, obtained as integrals of the real part of the Fourier Transform of corresponding FIDs. P_p is the calculated polarization of water phantom in B_{tot} in thermal equilibrium at ambient temperature, N_{Xe} and N_p

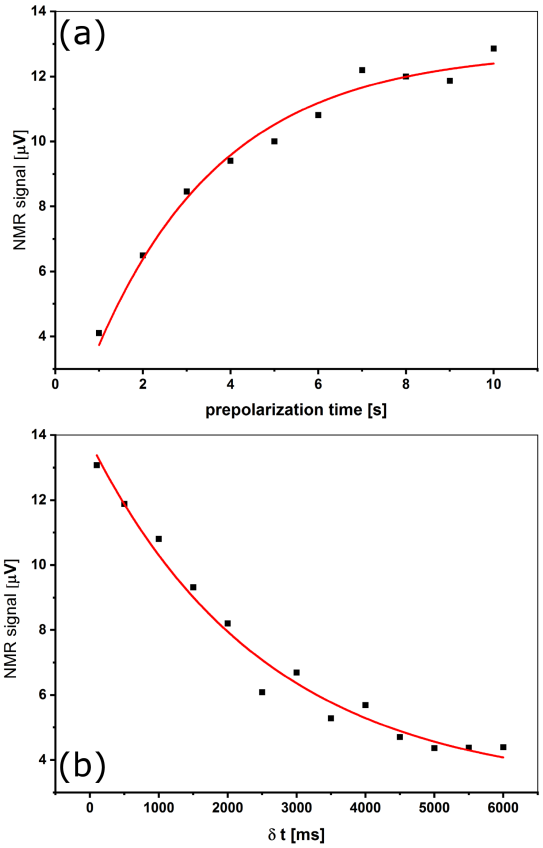

Fig. 6. Relaxation of water phantom in B_{tot} (a) and B_0 (b).

the numbers of xenon and proton nuclei in the measured volume, β_{129} the isotopic abundance of ^{129}Xe, and t_{del} is the dead time of the NMR receiver, which is equal to 1.5 ms. $T^*_{2,\mathrm{Xe}}$ and $T^*_{2,p}$ are the xenon and proton transverse relaxation times, respectively, including the magnetic field inhomogeneity effects. The N_{Xe} was calculated from the ideal gases law, and the number of protons is equal to:

$$N_p = \frac{2\rho_{\mathrm{H_2O}} V N_{\mathrm{Av}}}{M_{\mathrm{H_2O}}}, \tag{4}$$

where $\rho_{\mathrm{H_2O}}$ is the water density, V measured volume, N_{Av} Avogadro number, and $M_{\mathrm{H_2O}}$ molar mass of water.

Due to limited capabilities of the Prospa program, the directly sampled FID signal was transferred to Origin (Origin ver. 2017, OriginLab Corp.) for further processing. The implemented Digital Quadrature algorithm allowed for filtering, complex Fourier Transform (FT), phase correction, and integration of the real part of the spectrum.

5. Results

Two separate series of experiments were carried out. The first one aimed at achieving maximum possible polarization of xenon in a single step, while the second focused on producing large amounts of polarized xenon using the stop-flow mode.

5.1. Generation of the largest possible xenon polarization

In order to determine the optimal experimental conditions for a single OP cell filling mode, the following parameters were varied: xenon concentration in the gas mixtures (2 to 7.5 %), pressure inside the OP cell (0.95 to 1.25 bar), and the OP cell temperature (110 to 140 °C). The highest polarization was obtained with the parameters equal to 3 %, 1.2 bar, and 120 °C, respectively. A typical single pulse FT NMR spectrum of polarized xenon is shown in Fig. 7b, with the gas mixture proportions of ^{129}Xe:^{4}He:N_2 equal to 3.2:71.7:25.1. For comparison, Fig. 7a shows the spectrum of pre-polarized water phantom. The transverse relaxation times as determined from the envelope of the FID signal were $T^*_{2,Xe} = (15.1 \pm 1.3)$ ms and $T^*_{2,p} = (17.8 \pm 1.7)$ ms for xenon and protons, respectively. Using the Eq. (3), the absolute nuclear polarization of xenon was found to be $P_{\mathrm{Xe}} = (39 \pm 2.3)\%$. From the exponential build-up curve of xenon polarization which is shown in Fig. 8, the time constant $T_{\mathrm{build-up}} = (6.0 \pm 1.3)$ min was also calculated.

5.2. Producing large amount of hyperpolarized xenon in the stop-flow mode

In this case, it was necessary to find the best compromise between the xenon polarization level and production efficiency. Taking into account polarization losses due to

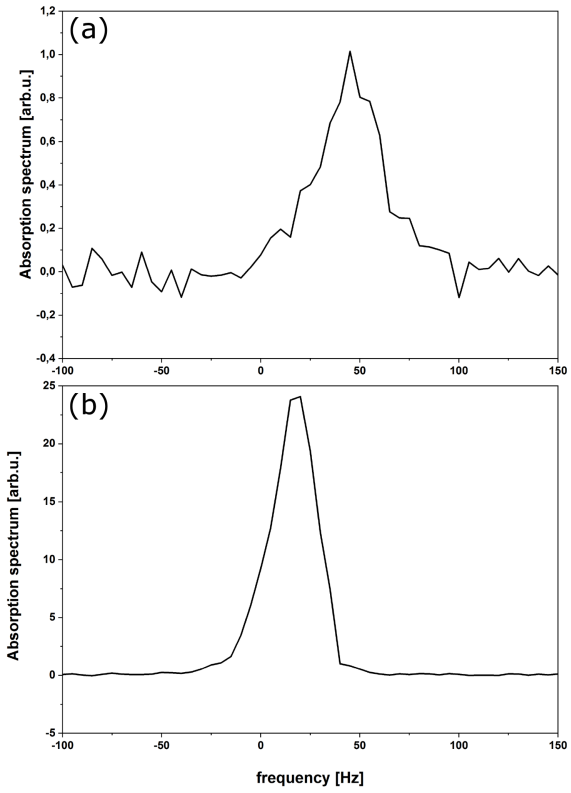

Fig. 7. FT NMR spectra of pre-polarized water phantom (a) and hyperpolarized xenon (b).

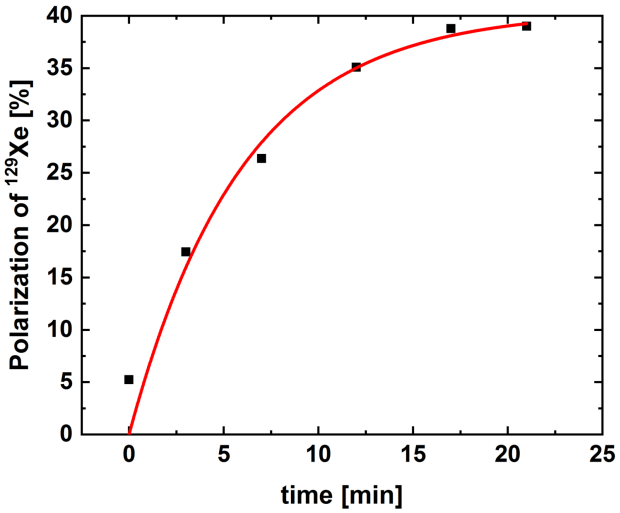

Fig. 8. Typical xenon polarization build-up curve.

relaxation processes during accumulation and storage, it was decided to accumulate five 60 cm^3 portions of moderately polarized xenon in about an hour. Each step consisted of 8 minutes of polarization and 4 minutes of xenon extraction and refilling OP cell with the new gas mixture. The xenon concentration in the gas mixture was increased to 6 %, resulting in the reduction of its final polarization to an average of 14.4 %, but allowing to accumulate 300 cm^3 of HP Xe in one hour. The frozen medium was transported in the cold finger inside the Halbach magnet and liquid nitrogen dewar to hospital in about 30 minutes.

A clinical 1.5 T Siemens Avanto medical MRI scanner that is installed in the John Paul II Hospital in Kraków was used in this experiment. An upgraded software and the dedicated for lung imaging birdcage coil purchased from Rapid Biomedical made it possible to operate the system at the ^{129}Xe resonance frequency equal to 17.6 MHz. A dedicated xenon phantom was used to tune the MRI scanner to the ^{129}Xe resonant frequency, determine the 90° RF pulse length, and calibrate the polarization of the hyperpolarized xenon. It was made of the 6 mm thick polycarbonate tube, which was filled with the 85 % (Cortecnet Europe) ^{129}Xe isotope enriched xenon gas at 9 bars and 1 bar of oxygen, to shorten the longitudinal relaxation time. The internal volume of the phantom equal to 566 cm^3 corresponded to 4330 scc of ^{129}Xe isotope. The phantom was thermally polarized by the magnetic field of medical scanner. According to the Eq. (2), the nuclear polarization of xenon at 295 K in 1.5 T was $P_{\mathrm{therm}} = 1.44 \times 10^{-6}$.

The cryogenic transport system for hyperpolarized xenon is shown in Fig. 9 (left), near the medical scanner room. Using the optimal route to minimize depolarization effects, the cold finger containing frozen xenon was transferred to the medical scanner magnet bore. There it was immersed in hot water so that the thawed xenon expanded into 1 litre Tedlar bag. Subsequently the Tedlar bag was filled to up to 1 litre with pure nitrogen.

A single shot NMR experiment using the RF pulse with a flip angle of 10° was performed, and the resulting FT NMR spectrum is shown in Fig. 9 (right). The amplitude of hyperpolarized xenon line was about 700 times greater than from the xenon phantom, which is shown in Fig. 9 (middle). Taking into account the amount

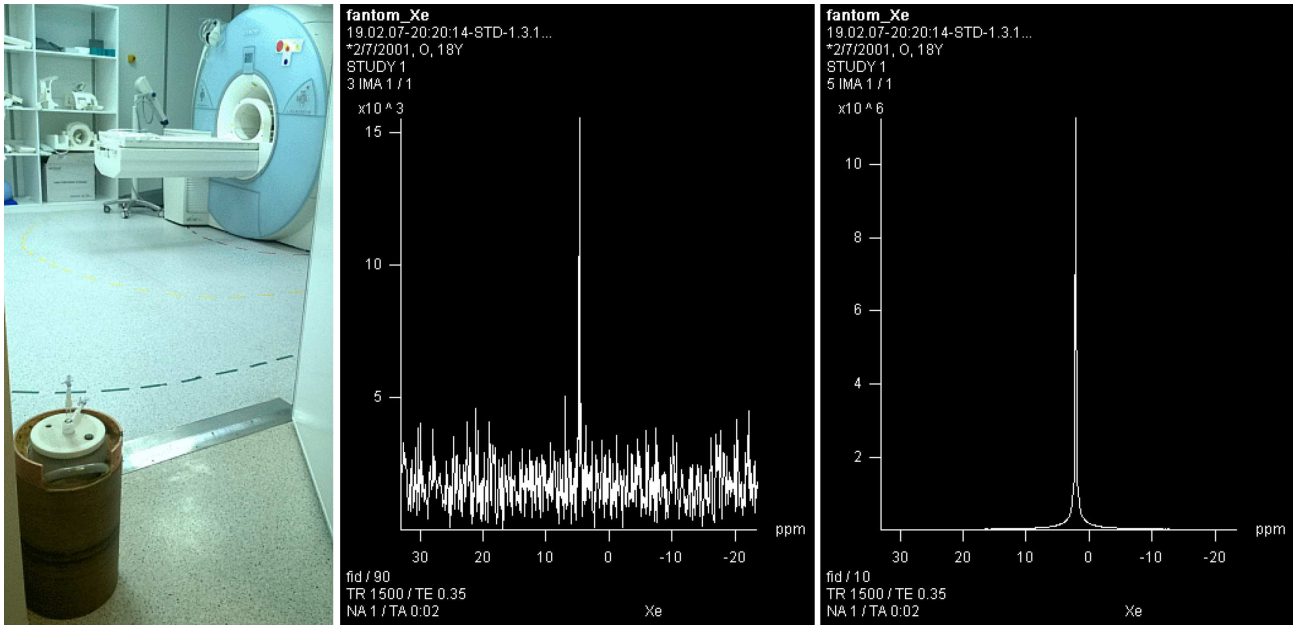

Fig. 9. HP Xe cryogenic transport system, (left); FT ^{129}Xe NMR spectrum of xenon in the phantom, 90° RF pulse, (middle) and in the Tedlar bag, 10° RF pulse, (right).

of ^{129}Xe in both containers, different RF pulse flip angles, and the calculated thermal polarization of xenon in the phantom, the nuclear polarization of the defrosted xenon was estimated to be about 9 %. This is the result of relaxation processes occurring during accumulation, storage, and transportation. A successful attempt was made to obtain the first MR image of the human lungs after inhalation with the gas portion described above, but it had a low quality. Therefore the improvement of accumulation and xenon thawing techniques is necessary.

6. Conclusions

The design and construction of the low cost SEOP ^{129}Xe polarizer operating in the stop-flow mode was described. Using a commercially available array of laser diodes with an external resonator, an optical system was made to form and polarize the laser beam. Despite the low laser power, which was about 9 W at the input of the OP cell, the nuclear polarization of ^{129}Xe reached a value of about 40 % in 1 litre of gas mixture containing 3 % isotopically enriched xenon, in the experiment made in a closed OP cell. The larger amount of HP Xe, as needed for lung MRI, was obtained by accumulation in the cold trap that was placed inside the 0.6 T Halbach magnet. The accumulation of five portions of polarized gas was carried out. The OP cell was filled with a gas mixture containing 6 % xenon. In one hour, a portion of 300 cm^3 of HP Xe was obtained. In a single accumulation step, the average xenon polarization was 14.4 %. After accumulation process, storage, transportation and defrosting, the polarization of HP xenon decreased to 9 %.

Further improvements of the system are planned to increase the polarization and amount of xenon obtained in the accumulation mode. First of all, a more powerful laser will be implemented, to shorten the SEOP process and increase the degree of polarization. Furthermore, the gas mixture preparation and dosing will be improved, to make the process more reproducible and to eliminate the rubidium oxidation effects. Furthermore, in order to reduce the xenon polarization losses during storage and transportation, the installation of the polarizer in the hospital is considered. The xenon defrosting process should be also improved so that HP Xe can be brought into high magnetic field of the MR scanner in the gas phase.

Acknowledgments

The project was supported by grants from: Polish National Centre for Research and Development, PBS3/A9/35/2015; National Laboratory for Quantum Technologies European Regional Development Fund, Innovative Economy Operational Program, WND-POIG.020200-00-003/08 and Jagiellonian University, Faculty of Physics, Astronomy and Applied Computer Science, K/DSC/004995. The authors would also like to thank Janusz Kuźma from the Institute of Physics of the Jagiellonian University for the design and construction of the diode laser and Roman Wiertek from the Institute of Nuclear Physics in Krakow for the design and construction of the Xe phantom and the heating chamber.

References

[1] *Hyperpolarized and Inert Gas MRI*, Eds. M.S. Albert, F. Hane, Academic Press, 2017.

[2] *Gas Phase NMR*, Eds. K. Jackowski, M. Jaszuński, Royal Society of Chemistry, 2016.

[3] *Hyperpolarized Xenon-129 Magnetic Resonance: Concepts, Production, Techniques and Applications*, Eds. T. Meersmann, E. Brunner, Royal Society of Chemistry, 2015.

[4] P. Peuravaara, J. Karjalainen, J. Zhu, J. Mareš, P. Lantto, J. Vaara, *Scientific Reports, Nature* **8**, 7023 (2018).

[5] B.M. Godson, *J. Magn. Res.* **155**, 157 (2002).

[6] G. Norquay, G. Leung, N.J. Stewart, G.M. Tozer, J. Wolber, J.M. Wild, *Magn. Reson. Med.* **74**, 303 (2015).

[7] E. Weiland, M.-A. Springuel-Huet, A. Nossov, A. Gédéon, *Micropor. Mesopor. Mater.* **225**, 41 (2016).

[8] J.P. Mugler III, T.A. Altes, *J. Magn. Reson. Imaging* **37**, 313 (2013).

[9] N.J. Stewart, H. F. Chan, P.J.C. Hughes, F.C. Horn, G. Norquay, M. Rao, D.P. Yates, R.H. Ireland, M.Q. Hatton, B.A. Tahir, P. Ford, A.J. Swift, R. Lawson, H. Marshall, G.J. Collier, J.M. Wild, *J. Magn. Reson. Imaging* **48**, 632 (2018).

[10] J.E. Roos, H.P. McAdams, S.S. Kaushik, B. Driehuys, *Magn. Reson. Imaging Clin. N Am.* **23**, 217 (2015).

[11] M.R. Rao, N.J. Stewart, P.D. Griffiths, G. Norquay, J.M. Wild, *Radiology* **286**, 659 (2018).

[12] M.R. Rao, N.J. Stewart, G. Norquay, P.D. Griffiths, J.M. Wild, *Magn. Reson. Med.* **75**, 2227 (2016).

[13] W. Happer, E. Miron, S. Schaefer, D. Schreiber, W.A. van Wijngaarden, X. Zeng, *Phys. Rev. A* **29**, 3092 (1984).

[14] S. Appelt, A. Ben-Amar Baranga, C.J. Erickson, M.V. Romalis, A.R. Young, W. Happer, *Phys. Rev. A* **58**, 1412 (1998).

[15] T.G. Walker, W. Happer, *Rev. Mod. Phys.* **69**, 629 (1997).

[16] M. S. Rosen, T. E. Chupp, K. P. Coulter, R. C. Welsh, S. D. Swanson, *Rev. Sci. Instrum.* **70**, 1546 (1999).

[17] F.W. Hersman, I.C. Ruset, S. Ketel, I. Muradian, S.D. Covrig, J. Distelbrink, W. Porter, D. Watt, J. Ketel, J. Brackett, A. Hope, S. Patz, *Acad. Radiol.* **15**, 683 (2008).

[18] S.E. Korchak, W. Kilian, L. Mitschang, *Appl. Magn. Reson.* **44**, 65 (2013).

[19] P. Nikolaou, A.M. Coffey, L.L. Walkup, B.M. Gust, N. Whiting, H. Newton, I. Muradyan, M. Dabaghyan, K. Ranta, G.D. Moroz, M.S. Rosen, S. Patz, M.J. Barlow, E.Y. Chekmenev, B.M. Goodson, *Magn. Res. Imag.* **32**, 541 (2014).

[20] G. Norquay, G.J. Collier, M. Rao, N.J. Stewart, J.M. Wild, *Phys. Rev. Lett.* **121**, 153201 (2018).

[21] POLAREAN, Polarean 9820^{129}Xe Hyperpolarizer.

[22] Xemed, XeBox-E10.

[23] M.S. Albert, G.D. Cates, B. Driehuys, W. Happer, B. Saam, C.S. Springer Jr, A. Wishnia, *Nature* **370**, 199 (1994).

[24] H.U. Kauczor, D. Hofmann, K.F. Kreitner, H. Nilgens, R. Surkau, W. Heil, A. Potthast, M.V. Knopp, E.W. Otten, M. Thelen, *Radiology* **201**, 564 (1996).

[25] M. Ebert, T. Grossmann, W. Heil, W.E. Otten, R. Surkau, M. Leduc, P. Bachert, M.V. Knopp, L.R. Schad, M. Thelen, *Lancet* **347**, 1297 (1996).

[26] J.R. MacFall, H.C. Charles, R.D. Black, H. Middleton, J. C. Swartz, B. Saam, B. Driehuys, C. Erickson, W. Happer, G.D. Cates, G.A. Johnson, C.E. Ravin, *Radiology* **200**, 553 (1996).

[27] G.D. Cates, R.J. Fitzgerald, A.S. Barton, P. Bogorad, M. Gatzke, N.R. Newbury, B. Saam, *Phys. Rev. A* **45**, 4631 (1992).

[28] N.D. Bhaskar, W. Happer, T. McClelland, *Phys. Rev. Lett.* **49**, 25 (1982).

[29] J. Fukutomi, E. Suzuki, T. Shimizu, A. Kimura, H. Fujiwara, *J. Magn. Reson.* **160**, 26 (2003).

[30] H. Imai, J. Fukutomi, A. Kimura, H. Fujiwara, *Concepts Magn. Reson. Part B (Magn. Reson. Eng.)* **33B**, 192 (2008).

[31] A. Fink, D. Baumer, E. Brunner, *Phys. Rev. A.* **72**, 053411 (2005).

[32] N. Whiting, P. Nikolaou, N.A. Eschmann, B.M. Goodson, M.J. Barlow, *J. Magn. Reson.* **208**, 298 (2011).

[33] M.S. Freeman, K. Emami, B. Driehuys, *Phys. Rev. A* **90**, 023406 (2014).

[34] N. Whiting, P. Nikolaou, N.A. Eschmann, M.J. Barlow, R. Lammert, J. Ungar, W. Hu, L. Vaissie, B.M. Goodson, *Appl. Phys. B* **106**, 775 (2012).

[35] A. Wojna-Pelczar, Ph.D. thesis, Jagiellonian University in Kraków, 2015.

[36] W.J. Cummings, O. Hausser, W. Lorenzon, D.R. Swenson, B. Larson, *Phys. Rev. A* **51**, 4842 (1995).

[37] B. Chann, E. Babcock, L.W. Anderson, T.G. Walker, W.C. Chen, T.B. Smith, A.K. Thompson, T.R. Gentile, *J. Appl. Phys.* **94**, 6908 (2003).

[38] P. Nikolaou, N. Whiting, N.A. Eschmann, K.E. Chaffee, B.M. Goodson, M.J. Barlow, *J. Magn. Reson.* **197**, 249 (2009).

[39] B.L. Volodin, S.V. Dolgy, E.D. Melnik, E. Downs, J. Shaw, V.S. Ban, *Opt. Lett.* **29**, 1891 (2004).

[40] H.G. Treusch, R. Pandey, in: *High-Power Laser Handbuch*, Eds. H. Injeyan, G.D. Goodno, McGraw-Hill, New York 2011, p. 133.

[41] B. Driehuys, G.D. Cates, E. Miron, K. Sauer, D.K. Walter, W. Happer, *App. Phys. Lett.* **69**, 1668 (1996).

[42] R. Bjørk, *J. App. Phys.* **109**, 013915-7 (2011).

[43] S. Samayak, H. Heidari, in: *2017 IEEE SENSORS, Glasgow*, ICSENS, 2017 p. 8233894.

[44] D. Meeker, FEMM program, ver. 4.2.